Technical University of Denmark

DTU

The transition to chaotic phase synchronization

Mosekilde, Erik; Laugesen, Jakob Lund; Zhusubaliyev, Zh. T.

Link back to DTU Orbit

DTU Library
Technical Information Center of Denmark

The transition to chaotic phase synchronization

E. Mosekilde, J. L. Laugesen, and Zh. T. Zhusubaliyev

Additional information on AIP Conf. Proc.

Journal Homepage: http://proceedings.aip.org/

Journal Information: http://proceedings.aip.org/about/about_the_proceedings

Top downloads: http://proceedings.aip.org/dbt/most_downloaded.jsp?KEY=APCPCS

Information for Authors: http://proceedings.aip.org/authors/information_for_authors

The transition to chaotic phase synchronization

E. Mosekilde*, J. L. Laugesen* and Zh. T. Zhusubaliyev†

*Department of Physics, The Technical University of Denmark, 2800 Lyngby, Denmark
†Department of Computer Science, South West State University, 50 Years of October Str., 94, Kursk 305040, Russia

Abstract. The transition to chaotic phase synchronization for a periodically driven spiral-type chaotic oscillator is known to involve a dense set of saddle-node bifurcations. By following the synchronization transition through the cascade of period-doubling bifurcations in a forced Rössler system, this paper describes how these saddle-node bifurcations arise and how their characteristic cyclic organisation develops. We identify the cycles that are involved in the various saddle-node bifurcations and descibe how the formation of multi-layered resonance cycles in the synchronization domain is related to the torus doubling bifurcations that take place outside this domain. By examining a physiology-based model of the blood flow regulation to the individual functional unit (nephron) of the kidney we demonstrate how a similar bifurcation structure may arise in this system as a response to a periodically varying arterial blood pressure. The paper finally discusses how an alternative transition to chaotic phase synchronization may occur in the mutual synchronization of two chaotically oscillating period-doubling systems.

Keywords: Chaotic phase synchronization, torus-doubling, multi-layered tori, nephron autoregulation, physiology-based modeling
PACS: 05.45-a, 05.45 xt, 87.19 rh, 87.64 Aa

INTRODUCTION

Chaotic phase synchronization [1, 2, 3] denotes an interesting form of synchronization in which a chaotic oscillator adjusts the frequencies of its internal dynamics to the rhythm of an external forcing, or to the dynamics of another chaotic oscillator, while the amplitudes continue to vary in an irregular fashion. In a numerical experiment one can observe [4, 5, 6, 7] how the main frequency of a periodically driven chaotic oscillator varies with some control parameter until the system enters a region of synchronization where the main frequency remains constant and equal to the forcing frequency. The width of the mode-locking interval typically increases with the forcing amplitude and, as the system leaves this interval, its main frequency again starts to change.

Chaotic phase synchronization has been observed in a broad range of different physical, technical and biological systems, including a plasma discharge tube paced with a low amplitude wave generator [8], an array of coupled electronic oscillators [9], and a pair of interacting functional units of the kidney [10]. The transition between phase-locked and un-locked states represents a significant change in behavior, and we have previously suggested that transitions between different synchronization states among oscillatory biological processes may represent an important component in the normal physiological regulation of the living organism [10].

Over the years, chaotic phase synchronization has been the focus of considerable theoretical interest [11, 12, 13], and concepts and methods developed through this

work have been used to interpret mode-locking phenomena in data from many different sources. Along with changes in the variation of the average frequency, the transition between phase-locked and un-locked chaos is also reflected in a specific variation of the Lyapunov exponents, in characteristic changes of the spectrum of the forced chaotic oscillator, and through changes in the size and form of its Poincaré section [14, 15]. It is generally known that the edge of the synchronization domain is made up by a dense set of saddle-node bifurcations [6, 13, 16, 17]. However, several details of how this set arises, how it is organized, and how the transition to the ergodic torus that exists outside the resonance zone takes place appear not yet to have been worked out.

A main contribution in this direction is the theory of cyclic (or C-type) criticality developed by Kuznetsov *et al.* [18, 19, 20]. In particular these authors have shown that the period-doubling transition to chaos along the edge of a resonance tongue displays an unusual scaling behavior that involves pairs of subsequent period-doubling bifurcations. In order to examine the bifurcation structure in more detail, we have recently performed a continuation analysis of the involved transitions [21, 22, 23]. This has demonstrated how the dynamics of the periodically forced Rössler system develops through continued period-doubling bifurcations of both the node and the saddle cycles in a direction transverse to the original resonance torus, thus producing a system of so-called multi-layered resonance tori [21]. To delineate the range of existence of the period-doubled cycles, a new saddle-node bifurcation emerges on both sides of the resonance zone in each period-doubling bifurcation. For a particular side of the resonance tongue, these saddle-node bifurcations alternatingly arise from the stable and the unstable branch of the period-doubling curve, hence producing the characteristic cyclic structure of the criticality where the scaling relates to pairs of subsequent period-doubling bifurcations. Moreover, the new saddle-node bifurcation curves arise close to, but not in the so-called fold-flip bifurcation points where the period-doubling curves are tangent to the former saddle-node bifurcation curves. Additional bifurcations are therefore required to close the 'holes' between the saddle-node bifurcation curves.

By following the synchronization transition for the forced Rössler system from the region where the oscillator displays simple periodic dynamics and all the way up through the cascades of period-doubling bifurcations to the regime of chaos, the present paper describes how the saddle-node bifurcations arise and how they are arranged [21, 24]. We explain how the bifurcating modes are organized and determine at which of the many saddle-node bifurcation curves, the ergodic torus that exists outside the resonance domain is born. This leads to a discussion of how the torus doubling bifurcations that take place outside of the resonance zone are related to the transitions that occur in the synchronization domain.

By examining the bifurcation structure of a physiology-based model of the blood flow regulation to the individual functional unit (nephron) of the kidney, we demonstrate how the same type of critical behavior may occur in the nephron's response to a periodic variation in the arterial blood pressure [25]. We finally discuss a new type of transition from asynchronous to phase synchronized chaos that, besides the saddle-node bifurcations, also involves a dense set of torus bifurcation curves. This type of transition, that arises through interaction between a pair of period-doubling oscillators, has been observed both for coupled Rössler systems and for pairs of interacting nephrons [26].
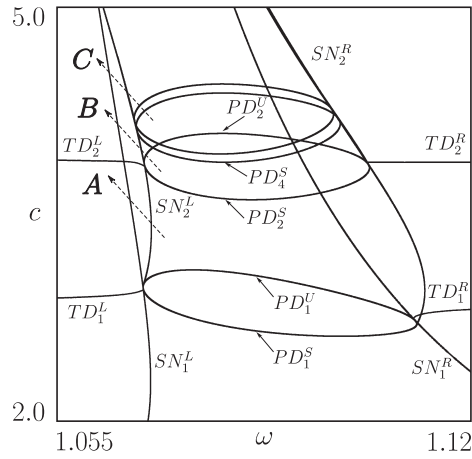
277

FIGURE 1. Two-dimensional bifurcation diagram for the 1:1 resonance zone of the periodically forced Rössler oscillator (1). ω and c represent, respectively, the forcing frequency and the nonlinearity parameter of the unforced Rössler oscillator. PD^S and PD^U denote period-doubling bifurcation curves for stable (node) and unstable (saddle) cycles, respectively. SN denotes saddle-node bifurcation curves, and TD locates torus doubling bifurcations outside the resonance zone. The arrows A, B and C define scan lines to be examined below. The figure was constructed by means of conventional continuation methods applying the software provided by Doedel *et al.* [27]

CROSSING THE BOUNDARY OF SYNCHRONIZATION

Let us consider the periodically forced Rössler system

$$\dot{x} = -y - z + A\sin(\omega t); \quad \dot{y} = x + ay; \quad \dot{z} = b + z(x - c) \tag{1}$$

that has also formed the basis for many earlier investigations of chaotic phase synchronization [11, 12, 13]. Here x, y and z are the dynamical variables of the unforced oscillator, and $A\sin(\omega t)$ represents the externally applied forcing. The parameters a and b and the forcing amplitude A are kept constant at the values $a = b = 0.2$ and $A = 0.1$ while the nonlinearity parameter c and the forcing frequency ω are used as bifurcation parameters.

With the above parameter values, the unforced Rössler system undergoes a Hopf bifurcation at $c = 0.4$ and for increasing values of c, the system hereafter exhibits a Feigenbaum cascade of period-doubling bifurcations. When an external periodic forcing is applied in the regime of periodic oscillations, the Rössler system displays regions of quasiperiodic (two-mode) dynamics interrupted by a dense set of resonance zones where the internally generated periodic oscillations synchronize with the external forcing. The 1:1 resonance domain is by far the most prominent, and the purpose of the present paper is to examine the structures that arise in and near this tongue as a result of the interplay between synchronization and period doubling.

Figure 1 provides an overview of the first four period-doubling bifurcations in the 1:1 resonance tongue [24]. Below the first period-doubling bifurcation PD_1^S, the resonance zone is delineated to the left and the right by the saddle-node bifurcation curves SN_1^L and SN_1^R, respectively. In this region the system displays a stable, synchronized period-

1 cycle and a corresponding saddle solution, both situated on the closed invariant curve that represents the resonance torus. Along the lower curve PD_1^S, the stable period-1 cycle undergoes its first period-doubling bifurcation, while the saddle solution period doubles at the curve PD_1^U. At the edge of the resonance zone the two solutions merge, and period doubling occurs simultaneously. We notice, however, that the period-doubling transitions take place in a direction transverse to the closed invariant curve [21, 22]. The repeated period-doubling process of both the node and saddle resonant cycles in this way gives rise to the formation of multi-layered resonance tori, i.e., nested structures of interconnected resonance tori [21, 22].

Above the curve PD_1^U, the system displays a pair of period-1 saddle and doubly unstable node cycles together with a pair of period-2 saddle and stable node cycles. The region of synchronization for the period-2 cycles is not identical to that of the period-1 cycles. Hence, while the saddle-node bifurcation curves SN_1^L and SN_1^R continue up along the tongue edge in order to delineate the region of resonant period-1 dynamics, a new set of saddle-node bifurcation curves SN_2^L and SN_2^R are born to delineate the range of synchronized period-2 dynamics. These new saddle-node bifurcation curves originate from the period-doubling curve in which the corresponding mode is born, typically from points close to the fold-flip bifurcation points where the period-doubling curve is tangent to the former set of saddle-node bifurcation curves. However, there is a gap between the two saddle-node bifurcation curves, and a variety of local and global bifurcations are called upon to close the hole and complete the border of the resonance zone [24].

The saddle-node bifurcation curves SN_2^L and SN_2^R are tangent to the next pair of period doubling curves. The stable period-2 solution undergoes a second period-doubling at PD_2^S, and the saddle period-2 solution period doubles at PD_2^U. As the value of c continues to increase, the same process repeats itself until the system undergoes a transition to phase synchronized chaos. This explains the build-up of a complete set of saddle-node bifurcation curves along the edges of the synchronization domain: A new pair of saddle-node bifurcation curves is generated for each pair of period-doubling bifurcations in order to delineate the region of existence for the newborn cycles. After the next pair of period-doubling bifurcations, the saddle-node bifurcation curves become curves at which the produced saddle and doubly unstable node cycles merge and disappear. In the interior of the resonance tongue, the period-doubling cascade for the node solutions progresses much faster than the same cascade for the saddle-cycles, and the transition to phase synchronized chaos takes place before the latter cascade in completed.

As first described by Arnéodo *et al.* [28] and by Kaneko [29], the ergodic torus undergoes a series of torus-doubling bifurcations along the edge of the resonance zone. More recently, this line of research has been persued by Sekikawa *et al.* [30, 31] who demonstrated a transition to chaos through a series of subsequent torus-doubling bifurcations both for an electric oscillator system and for a pair of coupled one-dimensional maps. As illustrated in Fig. 1, where the first two torus-doubling bifurcation curves are denoted TD_1 and TD_2, the torus-doubling bifurcations are coupled directly to the period-doubling bifurcations and, hence, to the formation of multi-layered resonance tori in the synchronization tongue. In this way, the ergodic torus always displays the same periodicity as the resonance torus it couples to across the synchronization edge. Below the first period-doubling bifurcation, the period-1 ergodic torus ends in a bifurcation (SN_1^L
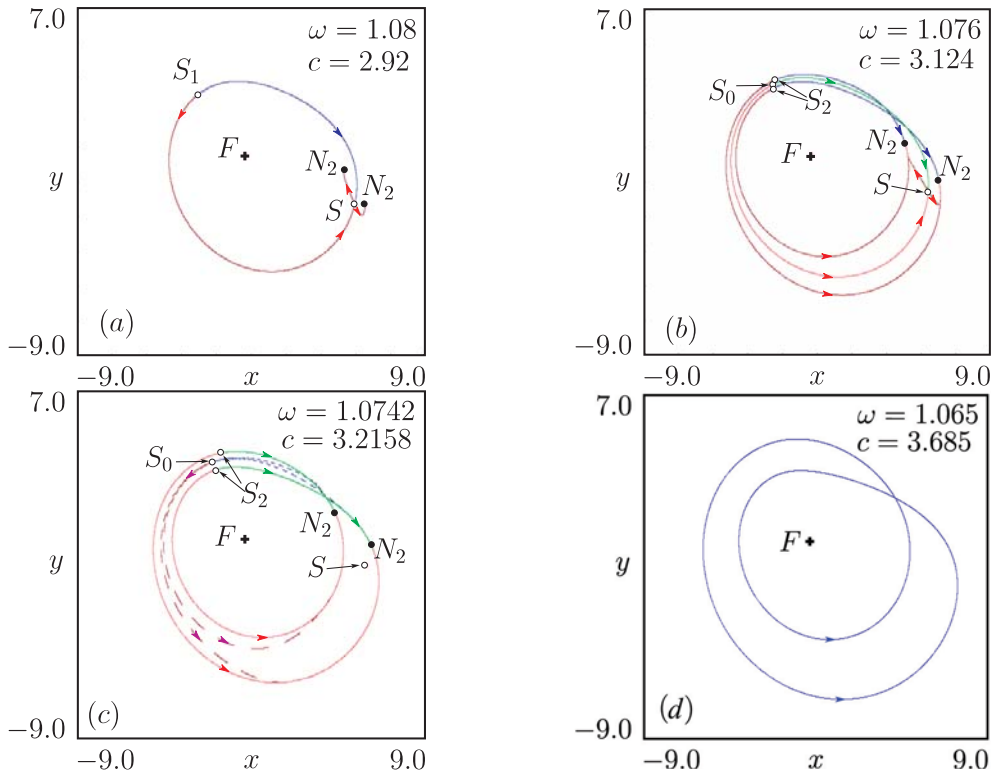
FIGURE 2. Different stages in the transition from 1:1 resonance torus to period-doubled ergodic torus along the scan A in Fig. 1 ($c = -51\omega + 58$). (a) Phase portrait after the period-doubling bifurcation of the stable node transversely to the 1:1 resonance torus. Here S_1 and S are resonant period-1 saddle solutions and N_2 is a stable period-2 node cycle. (b) Double-layered resonance torus that arises through a period-doubling bifurcation of the original period-1 saddle cycle S_1. S_0 is a doubly unstable period-1 cycle with multipliers $\rho_1 = -1.015$, $\rho_2 = 1.089$, $\rho_3 = -7.61 \cdot 10^{-8}$. (c) Destruction of the period-1 resonance torus. The two resonance cycles S_0 and S continue to exist but their unstable manifolds connect to the stable period-2 resonance cycle. (d) Period-2 ergodic torus that arises when the system leaves the resonance tongue along the direction A in Fig. 1.

or SN_1^R) that creates a pair of period-1 node and saddle cycles. Between the first and the second period-doubling bifurcation, the period-2 ergodic torus ends in a pair of period-2 node and saddle cycles along SN_2^L (or SN_2^R).

As an illustration to this description, Fig. 2 shows a number of stages in the transition through which the period-doubled ergodic torus arises from the period-1 resonance torus as the parameters are scanned along the direction A in Fig. 1. Starting at a point after the first period-doubling curve PD_1^S, Fig. 2(a) shows how the originally stable 1:1 resonance cycle has undergone a period-doubling bifurcation in a direction transverse to the synchronization manifold, i.e., the unstable manifold of the 1:1 resonance saddle S_1. While giving birth to the stable 2:2 resonance cycle N_2, the period-doubling bifurcation has left the original 1:1 node as a saddle cycle with its unstable direction transverse to the synchronization manifold. When crossing the period-doubling bifurcation curve PD_1^U in Fig. 1, the original 1:1 resonance saddle also undergoes a transverse period-doubling bifurcation, leading to the 2:2 resonance saddle S_2 and the doubly unstable
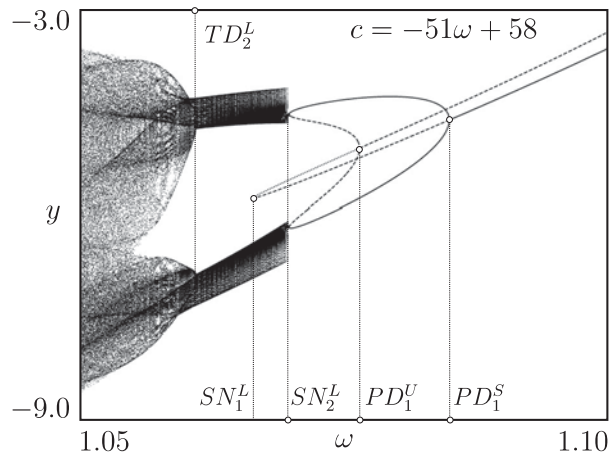
FIGURE 3. One-dimensional scan along the direction A in Fig. 1. The pair of saddle and doubly unstable 1:1 resonance cycles merge and disappear in SN_1^L. The pair of saddle and stable 2:2 cycles merge in SN_2^L, leading to a period-2 ergodic torus. The ergodic period-2 torus subsequently undergoes a torus-doubling at TD_2^L.

resonance cycle S_0 (Fig. 2(b)). This latter transition gives birth to a so-called double-layered torus [21, 22, 24], i.e. a structure of interconnected layers of stable and unstable tori. As the scan continues the period-1 resonance torus is destroyed (Fig. 2(c)) and, as the system crosses through the saddle-node bifurcation curves SN_2^L and SN_1^L, we observe first how the 2:2 saddle and stable node cycles merge and disappear through the birth of a period-doubled ergodic torus at SN_2^L and, thereafter, how the pair of 1:1 saddle and doubly unstable node cycles merge and disappear in the saddle-node bifurcation SN_1^L leading to a period-2 ergodic torus (Fig. 2(d)).

If the scan is continued one can observe how the ergodic torus undergoes a second torus doubling at the bifurcation curve TD_2^L in Fig. 1. This is illustrated in the one-dimensional bifurcation diagram of Fig. 3 which again shows the transitions that take place along the direction A in Fig. 1. Full curves represent stable periodic cycles, dashed curves saddle cycles, and dotted curves doubly unstable node solutions. Notice how the stable 1:1 solution that exists in the upper right corner of the figure undergoes a period-doubling at PD_1^S while the corresponding 1:1 saddle solution suffers its first period doubling at PD_1^U. From here we can follow the two solutions (now as a saddle cycle and a doubly unstable node) to the saddle-node bifurcation SN_1^L to the left in the figure. This saddle-node bifurcation defines the zone edge for the period-1 cycles. The saddle and stable node 2:2 resonance cycles merge at SN_2^L to give birth to a period-doubled ergodic torus. Finally, when crossing the torus-doubling bifurcation curve TD_2^L, the ergodic torus undergoes a new period-doubling transition.

Figure 4 shows a similar one-dimensional bifurcation diagram for the direction B in Fig. 1. After the first period-doubling bifurcations for the 1:1 resonance node and saddle cycles at PD_1^S and PD_1^U, the interconnected period-doubling processes continue to the left in the figure. Here we can locate the period-doubling bifurcation PD_2^S for the stable period-2 cycle and the bifurcation PD_2^U for the corresponding saddle cycle. Each pair of
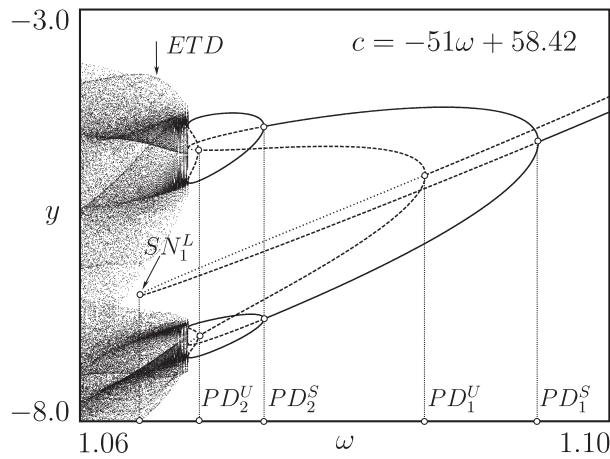
FIGURE 4. One-dimensional scan along the direction B in Fig. 1. As the forcing frequency ω is reduced, the resonant period-4 torus ends in a saddle-node bifurcation that gives birth to a period-4 ergodic torus. The torus-doubling process only occurs in a restricted region on both sides of the resonance tongue. At the point ETD, this ergodic torus is destroyed, and to the left of ETD the system displays non-synchronous chaos.
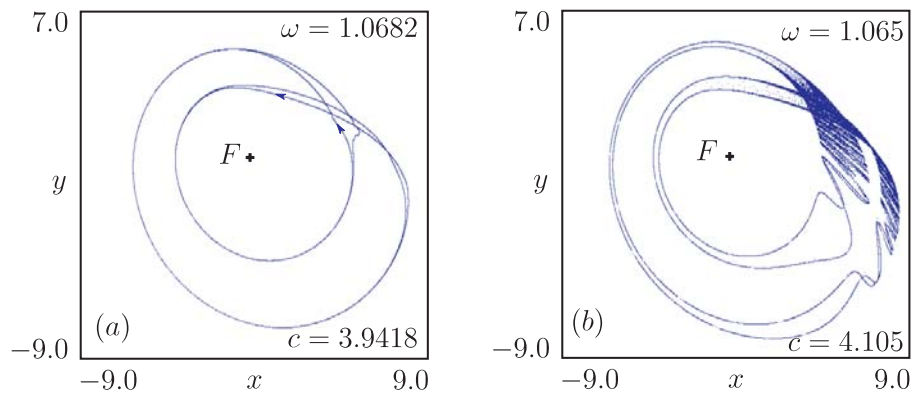

FIGURE 5. The process of ergodic torus destruction. (a) Cross section of the period-4 ergodic torus that exists to the right of the threshold ETD in Fig. 4. (b) Non-synchronous chaotic attractor to the left of ETD.

saddle and doubly unstable node cycles born in these bifurcations can subsequently be followed to the saddle-node bifurcation that demarcates their synchronization zone.

In Fig. 4, the boundary of the resonance zone consists of saddle-node bifurcations for the period-1, period-2, and period-4 cycles, but only the period-4 node is stable, and both the 1:1 and the 2:2 resonance tori have been destroyed. Hence, we observe that the period-4 resonance torus ends in a saddle-node bifurcation in which an ergodic period-4 torus is born. The period-1 saddle and doubly unstable node cycles continue to exist into the region of the stable period-4 ergodic torus. As the system moves further away from the resonance zone, the ergodic torus starts to fold and it finally undergoes torus destruction at the point ETD where its different layers begin to mix.

Figures 5 (a) and (b) provide an illustration to the ergodic torus destruction process.
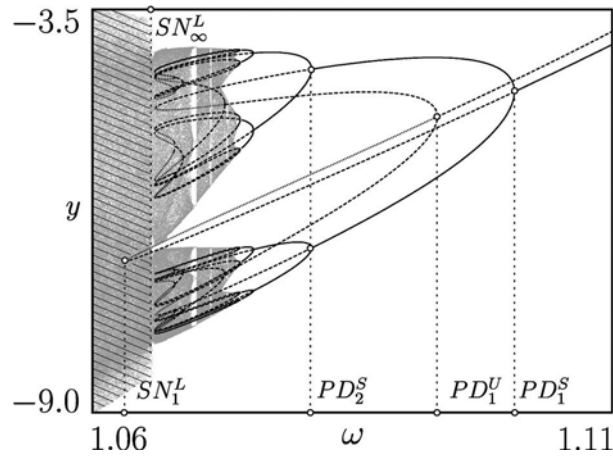
FIGURE 6. Bifurcation diagram along the scan line C in Fig. 1. Each pair of saddle and doubly unstable node cycles generated in the period-doubling bifurcations merge in a specific saddle-node bifurcation along the edge of the resonance zone. The figure also illustrates the transition from phase-locked chaos (dotted) to non-synchronous chaos (hatched) at the point SN_∞^L.

Here we have plotted a Poincaré section of the period-4 ergodic torus that exists to the right of the point ETD in Fig. 4 together with a similar section and of the non-synchronized chaotic attractor that arises when the threshold of torus destruction is crossed. As one would expect, the transition from ergodic torus dynamics to non-synchronous chaos is accompanied by one of the Lyapunov exponents turning positive.

Finally, Fig. 6 shows a one-dimensional bifurcation diagram along the scan line C in Fig. 1. Here, $c = -51\omega + 58.75$, and the scan takes the system from the region of period-1 resonance all the way through the regime of phase synchronized chaos and out across the edge of the resonance zone. With decreasing values of ω, the state of phase-synchronized chaos is reached when the stable resonance cycles have completed their period-doubling cascade. In Fig. 6 this region, as obtained from a normal brute-force bifurcation scan, is shown as a dotted structure. This allows us to also illustrate the appearance of periodic windows in the region of phase-synchronized chaos. With further decrease of ω, the doubly unstable modes arising through period-doubling of the saddle cycles also start to contribute to the chaotic state. Finally, a transition to non-synchronous chaos occurs at SN_∞^L. This transition is associated with the abrupt change of one of the Lyapunov exponents from being negative to becoming zero, hence resembling a normal saddle-node bifurcation between a resonant and an ergodic torus.

THE CYCLIC BIFURCATION STRUCTURE

Let us examine the above bifurcation scenario in a little more detail, focusing in particular on the problems that arise near the fold-flip bifurcation points, i.e., the points where a saddle-node bifurcation curve is tangent to a period-doubling curve and where a resonance cycle simultaneously undergoes a saddle-node and a period-doubling bifurcation [32].
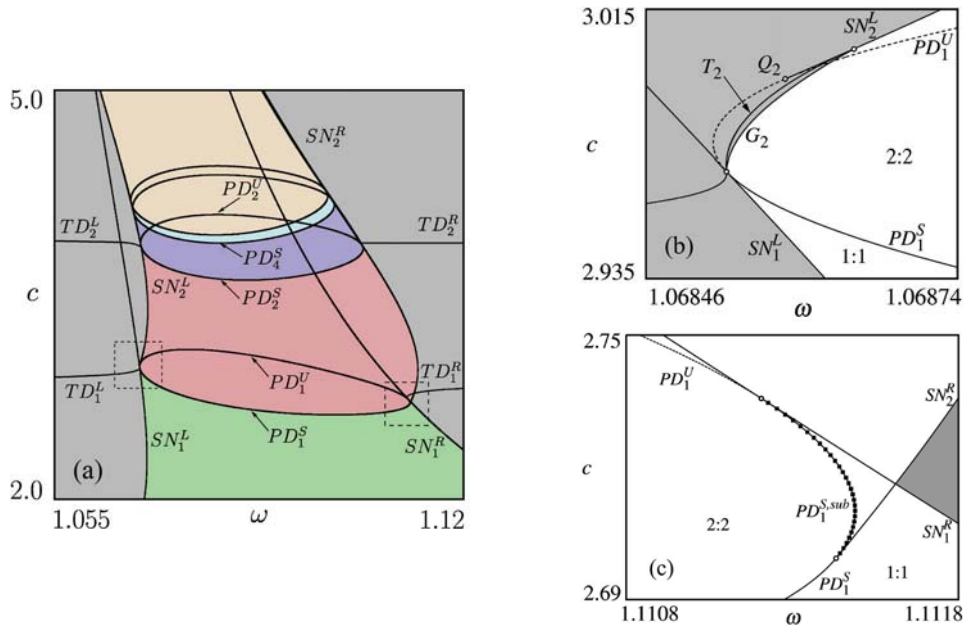
FIGURE 7. Bifurcation structure of the 1:1 Arnol'd tongue in the periodically forced Rössler system. (a) Overview of the first four period-doubling and saddle-node bifurcations. Only the first two pairs of saddle-node bifurcations are distinguishable at this scale. (b) Enlargement of the region around PD_1 and SN_1^L. The gap between the tangent point for SN_1^L and the point of birth for SN_2^L is closed by the subcritical torus-birth bifurcation T_2 in conjuction with a torus-fold bifurcation near to G_2. (c) Enlargement of the region around PD_1 and SN_1^R. SN_2^R is born on the stable branch PD_1^S, and part of the period-doubling curve is subcritical.

Figure 7(a) provides a slightly redrawn version of Fig. 1 in which the regions of existence for the stable 1:1, 2:2, 4:4, etc. resonance cycles are illustrated in different colors. Figures 7(b) and (c) show magnifications of the regions near the fold-flip bifurcation points where the saddle-node bifurcation curves SN_1^L, respectively SN_1^R, are tangent to the first period-doubling bifurcation curve PD_1. Inspection of Fig. 7(b) shows that the saddle-node bifurcation curve SN_2^L initiates from a point Q_2 on the unstable branch of PD_1 and close to the point of tangency between PD_1 and SN_1^L, but not exactly in that point. Numerical simulations have shown that the distance between the two points decrease with increasing forcing amplitude, but it continues to exist as long as the forcing amplitude is finite. This creates a hole in the boundary that defines the region of existence for the period-2 resonance cycles, and additional mechanisms are required in order to close this hole. As discussed in more detail in our recent work [24], these additional mechanisms involve:

i) a subcritical torus-birth bifurcation (secondary Hopf bifurcation) T_2 in which an unstable two-branch torus arises through destabilization of the stable period-2 resonance cycle (now of focus type).

ii) a torus-fold bifurcation (close to G_2 in Fig. 7(b)) in which a pair of stable and unstable period-doubled ergodic tori arise, and
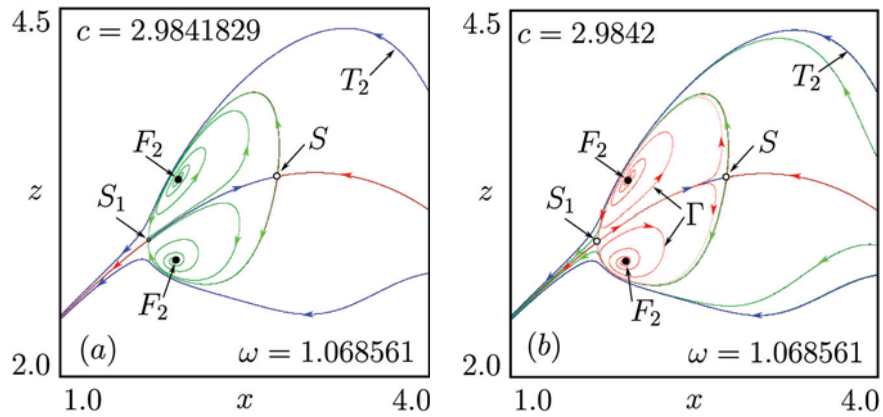
284

FIGURE 8. Heteroclinic bifurcation in which the unstable period-doubled ergodic torus is replaced by an unstable two-branch torus. (a) Immediately before the heteroclinic bifurcation ($c = 2.9841829$), the phase portrait displays a stable period-doubled ergodic torus T_2, an unstable period-doubled ergodic torus (not shown), and a stable period-2 focus cycle. The unstable manifold (green curve) of the period-1 saddle cycle S connects to F_2. (b) After the heteroclinic bifurcation ($c = 2.9842$), the unstable period-doubled torus has disappeared. The unstable manifold of S (green curve) now approaches T_2, and a new unstable two-branch torus has been formed around F_2. The red curve denoted Γ illustrates a trajectory that starts inside of the stable manifold of the unstable two-branch torus.

iii) a heteroclinic bifurcation (G_2) in which the unstable two-branch torus is transformed into the unstable period-doubled torus.

The combination of these mechanisms represents a way by which the stable period-2 cycle can be degraded to a doubly unstable period-2 cycle while at the same time a period-doubled ergodic torus is born. The doubly unstable period-2 cycle subsequently disappers in the period-doubling bifurcation at PD_1^U. In order for this to happen the period-doubling process takes a subcritical form in the interval from the point of tangency with SN_1 to Q_2 [24].

Figure 8 shows a couple of phase portraits in order to illustrate the heteroclinic bifurcation in which the unstable period-doubled torus disappears while at the same time an unstable two-branch torus is formed around the stable period-2 resonance cycle. Both phase portraits show the period-1 resonance torus with the original period-1 saddle cycle S_1 and the transversely unstable saddle cycle S produced in the period doubling at PD_1^S. Immediately before the heteroclinic bifurcation (Fig.8(a)), the unstable manifold of S (green curve) connects to the stable period-2 cycle F_2 of focus type. Surrounding this structure on alternating sides we observe the two bands of the period-doubled ergodic torus. The unstable period-doubled torus is not shown, but the stable manifold to S_1 arrives from the stable manifold of this torus.

The heteroclinic bifurcation involves the crossing of the unstable manifold of S and the stable manifold of S_1. This process is known to produce a variety of complex nonlinear phenomena [33]. However, after this range of dynamic complexity, the unstable period-doubled torus has disappeared, the unstable manifold of S (green curve) connects to the stable period-doubled torus T_2, and an unstable two-branch torus has formed around F_2. The red curve denoted Γ illustrates the course of a trajectory that starts im-
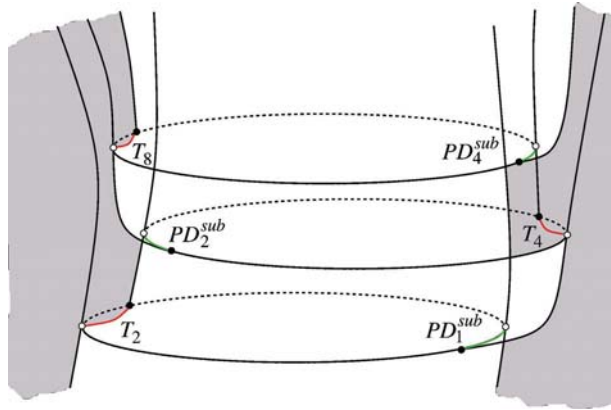
285

FIGURE 9. Sketch to illustrate the alternation of two different bifurcation scenarios in connection with the birth of new saddle-node bifurcation curves along the boundary of the resonance zone. The gray regions represent quasiperiodic dynamics outside the resonance zone.

mediately inside the unstable two-branch torus.

This completes our discussion of the bifurcation structure near the fold-flip bifurcation point for the case where the new saddle-node bifurcation curve emerge from the unstable branch of the period-doubling curve. The alternative situation where the saddle-node bifurcation emerges from the stable branch of PD_1, is observed on the other side of the resonance tongue. In this case, the new saddle-node bifurcation curve SN_2^R does not leave a gap through which the 2:2 resonance cycles can escape. However, to allow for that part of SN_2^R that falls below the point of intersection with SN_1^R (see Fig. 7(c)):

i) the section of the stable branch of PD_1 that connects the point in which SN_2^R is born with the point of tangency with SN_1^R must give rise to a subcritical period-doubling.

Moreover,

ii) while SN_2^R initially falls inside the already existing tongue structure, SN_2^R must intersect with SN_1^R and, at least over some distance, proceed outside the original resonance tongue.

Similar bifurcation phenomena take place near the fold-flip bifurcation points of the next period-doubling bifurcation, only the transition that involves a subcritical period-doubling bifurcation now occurs to the left, and the more complex transition involving different torus bifurcations occurs at the right hand side of the synchronization tongue. One would expect this process of alternation between the two sides of the resonance zone to continue from period-doubling to period-doubling. In a numerical study, Kuznetsov *et al.* [18, 19, 20] have shown that this is the case at least up to period-256. Hence, we may sketch the characteristic cyclic behavior of the bifurcation structure as illustrated in Fig. 9. Except for the first 2-3 bifurcations, saddle-node bifurcation curves emerging from the unstable branch of a period-doubling curve proceed inside the established resonance zone while, as argued above, saddle-node bifurcation curves that emerge from the stable branch of a period-doubling curve cross out of the existing resonance zone.

After this discussion we are left with the important question: Is there a specific
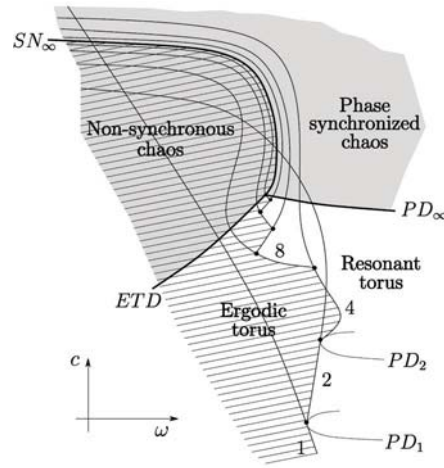
FIGURE 10. Sketch to illustrate the cascade of saddle-node bifurcation curves along the edge of the resonance zone. The curves denoted 1, 2 ,4, etc., represent the saddle-node bifurcation curves SN_1^L, SN_2^L, SN_4^L, etc. Note how the curves after an initial lack of organization begin to converge in an alternating fashion towards the final accumulation curve SN_∞. The hatched area represents the region of non-synchronous dynamics outside the resonance zone. PD_∞ represents the accumulation curve for the period-doubling cascade of the node cycles, and ETD is the curve of ergodic torus destruction.

organization of the saddle-node bifurcation curves along the edge of the resonance zone that continues all the way into the chaotic regime. This question has been answered in the affirmative by Kuznetsov *et al.* [18, 19, 20] through their formulation of a scaling theory for the transition to chaos via a cascade of period-doubling bifurcations along the edge of a synchronization tongue.

Figure 10 addresses the same question from a slightly different point of view. Here, we have plotted the saddle-node bifurcations that occur along the left hand side of the resonance tongue. While distorting the scales, this sketch strictly maintains the observed systematics of the variation. The curves denoted 1, 2, 4, 8, etc., represent the saddle-node bifurcation curves SN_1^L, SN_2^L, SN_4^L, etc.

Inspection of Fig. 10 shows that while the first few saddle-node bifurcation curves follow their own courses, a systematic arrangement is soon established in which the saddle-node bifurcation curves alternate between the two sides of what at the end becomes an accumulation curve SN_∞ for the saddle-node bifurcation curves. In the periodic region, i.e., the region below the transition to phase synchronized chaos, the ergodic torus is found to penetrate the cascade of saddle-node bifurcations along the edge of the resonance zone until it meets a stable periodic cycle. As illustrated in Fig. 10, where the region of non-synchronized dynamics to the left of the resonance domain is hatched, this implies that the transition from non-resonant to resonant dynamics at a given value of c always occurs along the saddle-node bifurcation curve that produces cycles with the highest periodicity.

The above bifurcation analysis has provided us with a coherent and more complete description of the many different phenomena that are involved in the transition to phase synchronized chaos via the route of C-type criticality. The purpose of the next sections is to show that similar phenomena can be observed in a detailed, physiology-based model

287

of nephron autoregulation.

PERIOD DOUBLING IN NEPHRON AUTOREGULATION

As part of an effort to understand the relation between hypertension and kidney function we have long been engaged with a study of nephron autoregulation, i.e., of the mechanisms by which the individual functional unit of the kidney regulates the incoming blood flow in response to variations in the arterial blood pressure [34, 35, 36]. This regulation involves two different mechanisms: A myogenic mechanism that reacts directly to changes in the arterial pressure, and a so-called tubuloglomerular feedback (TGF) mechanism that responds to signals from specialized cells (the macula densa cells) near the terminal part of the loop of Henle.

The myogenic mechanism depends on an inherent propensity of the smooth muscle cells in the arteriolar wall to contract in response to an increasing pressure difference across the wall [37, 38]. This contraction causes the flow resistance to increase and, thereby, leads to a lower glomerular pressure and a reduced rate of filtration. The TGF mechanism, on the other hand, depends on a response from the macula densa cells to changes in the salt concentration of the tubular fluid [39]. A high rate of glomerular filtration leads to a faster flow through the loop of Henle, to incomplete reabsorption of salt from the tubular fluid, rising salt concentrations at the macula densa, and a signal to the smooth muscle cells in the arteriolar wall to contract, thus causing the rate of filtration to decline.

The TGF mechanism is a negative feedback. However, as demonstrated in experiments on rats [40, 41], this mechanism tends to be unstable and to produce large amplitude self-sustained oscillations in the tubular pressures and flows with periods in the 30-40 sec range. The instability in the feedback and the relatively long periodicity of the oscillations are directly related to the time of 12-15 sec that it takes for the tubular fluid to pass the loop of Henle.

The myogenic (or vasomotoric) mechanism also produces oscillations in the afferent arteriolar resistance as the muscular activation increases. In this case, the transition to self-sustained oscillations takes place through synchronization of cytoplasmic Ca^{+2} waves among the individual cells [42, 43]. The period of the vasomotoric oscillations in the afferent arterioles of the kidney is typically 6-8 sec, or approximately a factor 5 shorter than the period of the TGF oscillations.

The two regulatory mechanisms both work through activation of the smooth muscle cells in the arteriolar wall. This allows the oscillatory modes to interact and to produce frequency-locking with typical locking ratios of 1:4, 1:5 and 1:6 [44, 45]. Nephron autoregulation involves a number of additional nonlinear relations that constrain the amplitudes of the oscillatory modes. Most important are the restrictions imposed by the limited dynamic range for the arteriolar contractions. This range can be determined through open loop experiments where the rate of glomerular filtration is measured as function of the rate at which artificial tubular fluid is infused into the loop of Henle, while preventing flow through the proximal tubule by means of a wax seal [39, 46]. The slope of this feedback characteristic determines the gain factor α for the TGF mechanism. This gain factor is typically 10-15 for normotensive rats and 30-50% higher for spontaneously

hypertensive rats. In general the sensitivity of the smooth muscle cells in the arteriolar wall is enhanced for hypertensive rats, and these rats also show a stronger interaction between the two oscillatory modes [44, 45].

Another important nonlinearity is represented by the static strain-stress relationship for the arteriolar wall. This relationship involves both a static component and an active vascular component. The static component increases almost exponentially with rising blood pressure and increasing arteriolar radius. The active component, on the other side, is most significant in a region around the normal arteriolar radius. By virtue of these and other nonlinearities, a range of different nonlinear dynamic phenomena are observed in the nephron pressures and flows. Period-2 dynamics for instance, is seen in about 50% of the experimental time traces for the proximal tubular pressure in normotensize rats and for hypertensive rats chaotic pressure and flow variations are typically observed [44, 45].

One this background, the purpose of the present section is to examine how the autoregulation of the blood flow to the individual nephron reacts to a periodic variation in the arteriolar blood pressure. In particular we want to show how the stable and unstable resonance cycles generated by such a forcing undergo interconnected cascades of period-doubling bifurcations and how each period doubling leads to the formation of a new pair of saddle-node bifurcation curves, in accordance with the bifurcation scenario for C-type criticality outlined in previous sections.

The ability of the renal autoregulation to handle external pressure fluctuations can be investigated by applying a forcing signal to the arterial pressure while simultaneously recording the variations observed in this pressure and in the renal blood flow. In practice, the experiment can be performed [47] by connecting a computer-operated pump that generates broadband fluctuations at the distal end of the abdominal aorta through a blood-filled cannula. The frequency characteristics observed in such an experiment clearly shows the damping of the pressure oscillations in the nephron blood flow at frequencies lower than 20 mHz.

Also revealed are the resonances characteristic of the autoregulatory system: the relatively slow TGF mode at about 40 mHz and the faster myogenic mode around 150 mHz. We conclude that the nephron autoregulation functions as a mechanical high-pass filter that protects the nephron against more long-term variations in the arterial pressure. Fluctuations above the range of the myogenic oscillations are likely to be damped out by various dissipative processes including those associated with the fluid flow through the loop of Henle. The TGF mechanism is unique to the nephrons and serves as a reinforcement of the myogenic mechanism in order to control the large blood flow that the kidney have to handle. The frequency response of the TGF mechanism is restricted, though, by the delay in the loop of Henle and, while reduced in amplitude by a factor of the order of two, the TGF oscillations are still present in the distal tubular pressure and salt concentration.

Over the years we have developed a number of different models of the regulation of the afferent blood flow by the individual nephron, each emphasizing a specific aspect of the problem such as the absorption of water and salts along the loop of Henle [48] or the interaction between the macula densa cells and the smooth muscle cells in the arteriolar wall [36]. In the present survey we will consider the model described by Barfred *et al.* [49]. This model integrates the most essential aspects of nephron autoregulation into a consistent picture and is, due to its simplicity, particularly useful for detailed bifurcation
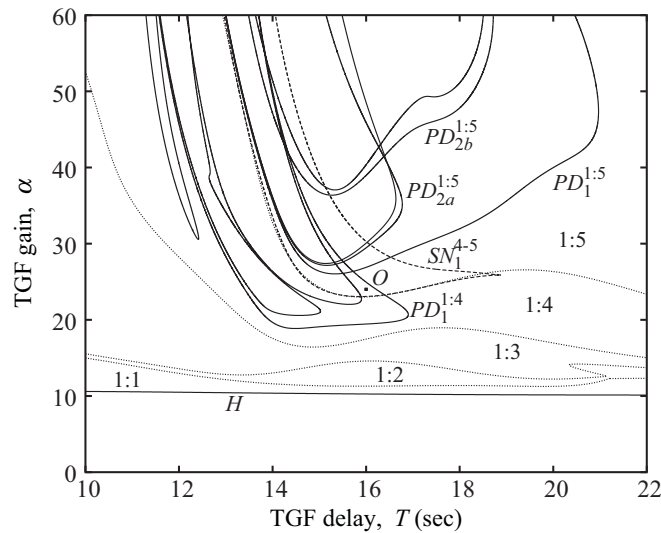
289

FIGURE 11. Two-dimensional bifurcation diagram for the unforced nephron model. The control parameters are the delay T and the gain factor α in the TGF regulation. The dotted curves delineate the regions of existence for different modes of entrainment between the fast myogenic and slower TGF-mediated oscillations. Fully drawn curves are period-doubling bifurcation curves and dashed curves are saddle-node bifurcation curves. The horizontal curve at $\alpha \approx 10$ is the Hopf bifurcation in which the TGF oscillations are born. The point O is the point of operation considered in the following investigation of the periodically forced nephron.

studies. The model involves six coupled differential equations and 20-30 experimentally determined parameters.

The first component in the model is a conservation equation that relates the changes in proximal tubular pressure to the rate of glomerular filtration, to the absorption that takes place in the proximal tubule, and to the flow into the loop of Henle. This is supported by an algebraic equation that determines the glomerular filtration in terms of the arterial pressure, the afferent arteriolar flow resistance, and the protein osmotic pressure of the incomming blod flow. The flow into the loop of Henle is determined by the pressure difference between the proximal and distal ends of this loop and the associated flow resistance, while the rate of reabsorption in the proximal tubule is treated as a constant.

The TGF mediated variation in the afferent arteriolar resistance is represented by the aforementioned open-loop feedback characteristic [39, 46]. A smooth delay is used to represent the time it takes for the nephron fluid to pass the loop of Henle, and a couple of first order differential equations are used to simulate the fast myogenic oscillations. In the form we use the model here these oscillations are damped, but continuously excited through the variations in the afferent arteriolar resistance caused by the TGF mechanism.

Figure 11 shows a two-dimensional bifurcation diagram for the unforced nephron model in a parameter plane spanned by the delay time T in the loop of Henle and the gain factor α for the TGF mechanism. Normal values for the feedback delay are about $T = 15$ sec and, as mentioned above, the feedback gain factor is typically $\alpha = 10 - 15$ for normotensive rats and some $30 - 50\%$ larger for spontaneously hypertensive rats.

290

However, other parameters also differ between the two strains of rats and it is, therefore, of interest to consider higher values of α where excitation of the myogenic oscillations becomes stronger.

The horizontal curve H at $\alpha \approx 10$ represents the Hopf bifurcation at which the onset of the TGF-mediated oscillations takes place. Below this curve, the nephron autoregulation displays a stable equilibrium point, and TGF-mediated oscillations do not occur. Experimentally, nephrons in normotensive rats are typically found to operate above, but relatively close to this threshold. The regions delineated by the dotted curves and denoted as 1:1, 1:2, 1:3, 1:4 and 1:5 represent the different regions of entrainment of the myogenic oscillations by the TGF-mediated oscillations. For small values of α, the myogenic dynamics lock directly into a 1:1 mode as one expects for a periodically driven oscillator at low amplitudes. As the gain factor increases, the excitation of the myogenic dynamics becomes stronger, and a shift to higher and higher excitation frequencies occurs. Double-wavelet analysis of the experimental data has confirmed that the most common frequency ratios under realistic conditions are 1:4 and 1:5 [44, 45], i.e. the myogenic mode completes four or five oscillations each time the slower TGF-mediated mode completes one full period.

The fully drawn curves in Fig. 11 represent period-doubling bifurcations. In the middle of the figure, for instance, we observe two cascades of period-doubling bifurcations denoted $PD_1^{1:5}$, $PD_{2a}^{1:5}$, $PD_{2b}^{1:5}$, etc., for the 1:5 mode-locked solution. At the curve $PD_1^{1:5}$, for instance, the synchronized 1:5 mode is replaced by a 2:10 mode in which the dynamics repeats itself only after two full TGF oscillations and 10 myogenic oscillations. We notice that mode-locking is maintained between the two oscillatory components during the period-doubling process. For slightly smaller values of the TGF delay, the 1:4 mode-locked solution is found to undergo similar cascades of period-doubling bifurcations. The dashed curve denoted $SN_1^{4:5}$ is a saddle-node bifurcation curve that delineates the region of coexistence between the 1:4 and 1:5 mode-locked solutions. In this region, depending on the initial conditions, the undisturbed model will approach a dynamics with either four myogenic oscillations per TGF oscillation or five myogenic oscillations per full cycle of the TGF oscillation.

The arterial pressure is a main determinant of the blood flow to the individual nephron and, as explained above, both the myogenic and the TGF-mediated regulation serve to reduce the impact of variations in the arterial blood pressure on the operation conditions of the nephron. It is therefore of interest to examine the response of our nephron model to a periodic variation in the arterial pressure:

$$P_a(t) = P_{a,0}(1 + A\sin(\omega t)) \tag{2}$$

$P_{a,0} = 13.3$ kPa is the mean arterial blood used to calculate the bifurcation diagram in Fig. 11. A denotes the relative amplitude of the applied forcing, and ω is the angular frequency.

At the chosen point of operation ($T = 16$ s and $\alpha = 25$, see Fig.11), the TGF generated self-sustained oscillations have a period of about 40 sec. This implies that only fluctuations in the arterial blood pressure that last for more than 80-100 sec can be effectively damped. Moreover, with the assumed values for T and α, the nephron operates in a regime where 1:5 and 2:8 mode-locking between the two internally generated frequen-
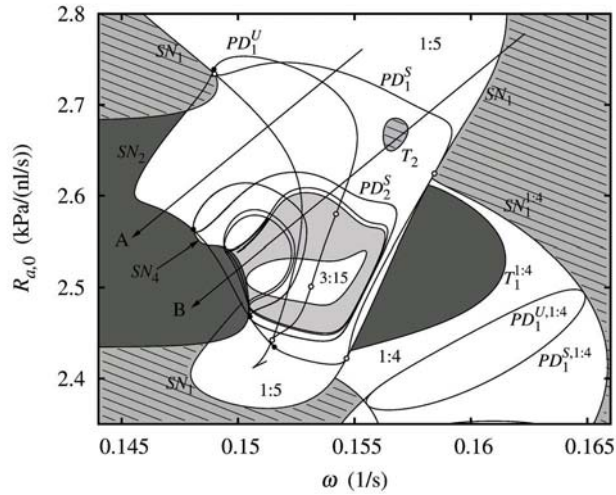
FIGURE 12. Two-dimensional bifurcation diagram for the forced nephron. Control parameters are the angular frequency ω of the forcing signal and the equilibrium value of the afferent arteriolar resistance $R_{a,0}$. White regions denote synchronized periodic dynamics, light grey regions phase-synchronized chaos, and dark grey regions represent non-synchronous chaos. The region where quasiperiodic dynamics occurs is hatched.

cies co-exist, the 2:8 solution being a period-doubled version of the 1:4 resonance cycle. To avoid mixing between the co-existing modes, or breaking up of the intra-nephron mode locking, we are restricted to use a fairly small forcing amplitude. In the following analysis, the forcing frequency is assumed to be close to the TGF frequency, and the constant forcing amplitude is $A = 0.0075$. Bifurcation parameters are the forcing frequency ω and the average arteriolar flow resistance $R_{a,0}$.

Figure 12 provides an overview of the bifurcation structure observed for the forced nephron model. We immediately notice that the diagram involves dynamic states deriving from both the 1:4 and the 1:5 states of intra-nephron synchronization. Moreover, both sets of dynamical states display synchronization with the applied forcing signal (white regions), period-doubling bifurcations, as well as transition to quasiperiodic dynamics (in the hatched regions). The 1:5 modes also display a transition to phase synchronized chaos (light gray region), and both modes display transitions to non-synchronous chaos (black regions).

As before period-doubling and saddle-node bifurcation curves are denoted PD and SN, respectively. For the period-doubling curves a superscript S denotes period-doubling of a stable (node) cycle and superscript U denotes period-doubling of an unstable (saddle) cycle. Bifurcations relating to 1:4 resonance modes have an additional superscript 1:4. This superscript has been omitted for the 1:5 modes. Torus bifurcation curves are denoted T.

The synchronized 1:4 resonance modes are observed in the lower right corner of the diagram. Here we notice the characteristic closed form of the first period-doubling curve $PD_1^{1:4}$ at which the synchronized 1:4 resonance node and saddle cycles undergo their first period-doubling bifurcation. This period-doubling curve is tangent on both sides to the saddle-node bifurcation curves $SN_1^{1:4}$ that delineate the range of existence for the
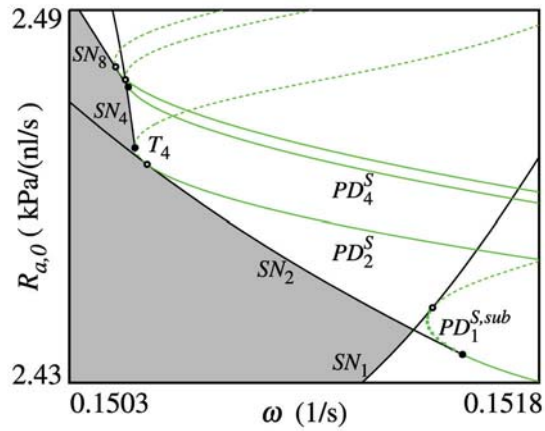
292

FIGURE 13. Close-up of the lower parts of the bifurcation structure in Fig. 12 for the forced nephron model. As usual gray and white regions denote respectively non-resonant and resonant dynamics. Like for the forced Rössler system the cascade of saddle-node bifurcation birth emerge alternatingly on the stable and unstable branch of the period-doubling curves.

1:4 resonance modes. As closer inspection shows, new saddle-node bifurcation curves emerge from the period-doubling curves in order to delineate the range of existence of the 2:8 resonance modes.

In the middle of Fig. 12, the large white area delineated along its right hand side by the saddle-node bifurcation curve SN_1 represents the area in which the 1:5 resonance modes produced by the nephron synchronize with the externally applied forcing signal. In the center of this area we find the region (denoted 3:15) where period-3 solutions to the original 1:5 resonance mode are observed. This region is surrounded by a light gray region with phase synchronized chaotic solutions, and this region is again surrounded by a cascade of period-doubling bifurcation curves. It is obvious that this structure is folded like a horse shoe such that period-doubling transitions to chaos take place along the left hand side of the resonance zone from both the top and the bottom.

A more detailed examination of the upper part of the 1:5 resonance zone shows how the stable 1:5 solution undergoes a period-doubling at PD_1^S while the corresponding saddle solution period doubles at PD_1^U. The two branches of this first period-doubling curve are tangent to the saddle-node bifurcation SN_1 in the upper left corner of the figure. A new saddle-node bifurcation curve SN_2 arises close to the point of tangency with PD_1, and this curve becomes tangent to the next period-doubling curve PD_2. Close to this point of tangency, a third saddle-node bifurcation curve SN_4 emerges, and the bifurcation structure continues in the same way as for the forced Rössler oscillator.

Figure 13 shows a close-up of the initial bifurcations for the lower period-doubling structure. Here, we can first identify the saddle-node bifurcation curve SN_1 that is tangent to the first period-doubling curve PD_1. The next saddle-node bifurcation curve SN_2 emerges from a point on the stable branch of PD_1, and the period-doubling associated with this branch becomes subcritical in the interval between the point of tangency with SN_1 and the point of birth for SN_2. The saddle-node bifurcation curve SN_2 is tangent to the next period-doubling curve PD_2. In this case, however, the new saddle-node

293

bifurcation curve SN_4 starts from a point on the unstable branch of PD_2. As a result, the gap between SN_2 and SN_4 is closed by a combination of a subcritical torus-birth bifurcation, a torus-fold bifurcation, and a variety of torus destruction processes.

CONCLUSIONS

Synchronization and other nonlinear dynamic phenomena play an essential role in the regulation of normal physiological systems. Regulation of the blood flow to the individual functional unit (nephron) of the kidney, for instance, involves both period-doubling bifurcations and intra-nephron synchronization of a fast (myogenic) and a slower (TGF-mediated) oscillation. Together these mechanisms serve as a mechanical filter that protects the delicate nephronic processes from the effect of more long term changes in the arterial blood pressure.

The purpose of the present paper has been to establish a more complete picture of the complex nonlinear dynamic phenomena that occur in connection with the transition to chaotic phase synchronization when a period-doubling oscillator of spiral type is subjected to a periodic forcing. Considering an externally forced Rössler oscillator we have first illustrated how the period-doubling transitions take place in a direction transverse to the synchronization manifold and how the period-doubling process leads to the formation of so-called multi-layered resonance tori, i.e., interconnected structures of stable and unstable tori of different periodicity.

It is well-known that the edge of the synchronization regime for a forced period-doubling oscillator consists of a large number of saddle-node bifurcation curves. By following the period-doubling transition step by step we have shown how these saddle-node bifurcation curves are arranged and how they emerge from points on the period-doubling curves close to the points where these curves are tangent to the saddle node bifurcation curves produced in the previous period-doubling process. Moreover, depending on whether the saddle-node bifurcation curves originate in the stable or the unstable branch of the period-doubling curve, different bifurcation scenarios are involved in closing the gap between the two saddle-node bifurcation curves. This explains the characteristic alternating (or cyclic) structure associated with C-type criticality.

We have also described how the period-doubling process in the resonance zone plays together with the period-doubling of the ergodic torus that takes place outside the resonance zone in order that the bifurcation at the zone edge always involves stable resonant and non-resonant tori of the same periodicity and form. This requires, for instance, that all unstable resonance tori are destructed before they reach the edge of the synchronization regime. However it also involves an interesting process by which:

i) A period-2 resonance cycle of focus type is destabilized in a subcritical torus-birth bifurcation and gives rise to an unstable two-branched ergodic torus,

ii) The unstable two-branched ergodic torus is transformed into an unstable period-doubled ergodic torus in a heteroclinic bifurcation, and

iii) The unstable period-doubled ergodic torus undergoes a torus-fold bifurcation and gives birth to a stable period-doubled torus.

We have hereafter demonstrated how a similar bifurcation structure occurs in the response of an individual nephron to a periodic variation in the arterial blood pressure. These results have recently been extended [26] by considering the bifurcation structure associated with the synchronization of two similar, but not identical period-doubling oscillators. Besides the formation in certain cases of new pairs of saddle-node bifurcation curves in each period-doubling bifurcation we have observed that this transition also involves the formation of torus bifurcation curves that continue up along the boundary of the resonance zone and accumulate in the region of phase synchronized chaos. Again, the findings from a system of two coupled Rössler oscillators are consistent with those of a pair of nephrons coupled through signals that travel along the connecting blood vessels (vascular propagated coupling).

ACKNOWLEDGMENTS

REFERENCES

1. V. S. Anishchenko, T. E. Vadivasova, D. E. Postnov, and M. A. Safonova, *Int. J. Bifur. Chaos* **2**, 633-644 (1992)
2. G. S. Dykman, P. S. Landa, and Yu. I. Neymark, *Chaos, Solitons and Fractals* **1**, 339-353 (1992)
3. P. S. Landa, and M. G. Rosenblum, *Appl. Mech. Rev.* **46**, 414-427 (1993)
4. M. G. Rosenblum, A. S. Pikovsky, and J. Kurths, *Phys. Rev. Lett.* **76**, 1804-1807 (1996)
5. N. F. Rulkov, *Chaos* **6**, 262-279 (1996)
6. A. S. Pikovsky, M. G. Rosenblum, G. V. Osipov, and J. Kurths, *Physica D* **104**, 219-238 (1997)
7. G. Osipov, A. Pikovsky, M. G. Rosenblum, and J. Kurths, *Phys. Rev. E* **55**, 2353-2361 (1997)
8. Jr. B. Rosa, W. B. Pardo, C. M. Ticos, J. A. Walkenstein, and M. Monti, *Int. J. Bifur. Chaos* **10**, 2551-2563 (2000)
9. A. Dabrowski, Z. Galias, and M. Ogorzalek, *Int. J. Bifur. Chaos* **10**, 2391-2398 (2000)
10. N.-H. Holstein-Rathlou, K.-P. Yip, O. V. Sosnovtseva, and E. Mosekilde, *Chaos* **11**, 417-426 (2001)
11. A. Pikovsky, M. Zaks, M. G. Rosenblum, G. Osipov, and J. Kurths, *Chaos* **7**, 680-687 (1997)
12. Jr. Rosa, E. Ott, and M. H. Hess, *Phys. Rev. Lett.* **80**, 1642-1645 (1998)
13. M. G Rosenblum, A. S. Pikovsky, and J. Kurths, *IEEE Trans. CAS-I* **44**, 874-881 (1997)
14. T. E. Vadivasova, A. G. Balanov, O. V. Sosnovtseva, D. E. Postnov, and E. Mosekilde, *Phys. Lett. A* **253**, 66-74 (1999)
15. D. E. Postnov, T. E. Vadivasova, O. V. Sosnovtseva, A. G. Balanov, V. S. Anishchenko, and E. Mosekilde, *Chaos* **9**, 227-232 (1999)
16. A. Pikovsky, M. Rosenblum, and J. Kurths, *Synchronization: A Universal Concept in Nonlinear Science*, Cambridge University Press, UK, (2001)
17. E. Mosekilde, Yu. Maistrenko and D. Postnov, *Chaotic Synchronization: Applications to Living Systems*, World Scientific, Singapore (2002)
18. S. P. Kuznetsov, A. P. Kuznetsov, and I. R. Sataev, *J. Stat. Phys.* **121**, 697-748 (2005)
19. S. P. Kuznetsov, A. P. Kuznetsov, and I. R. Sataev, *Physica D* **109**, 91-112 (1997)
20. S. P. Kuznetsov, and I. R. Sataev, *Phys. Rev. E* **64**, 046214-7 (2001)
21. Zh. T. Zhusubaliyev, J. L. Laugesen, and E. Mosekilde, *Phys. Lett. A* **374**, 2534-2538 (2010)
22. Zh. T. Zhusubaliyev, and E. Mosekilde, *Phys. Lett. A* **373**, 946-951 (2009)
23. Zh. T. Zhusubaliyev, and E. Mosekilde, *Physica D* **238**, 589-602 (2009)

24. J. L. Laugesen, E. Mosekilde, and Zh. T. Zhusubaliyev, *Physica D* **241**, 488-496 (2012)
25. J. L. Laugesen, E. Mosekilde, and N.-H. Holstein-Rathlou, *Interface Focus* **1**, 132-142 (2011)
26. J. L. Laugesen, E. Mosekilde, and N.-H. Holstein-Rathlou, *Chaos* **21**, 033128-12 (2011)
27. J. Doedel, R. C. Paffenroth, A. R. Champneys, T. F. Fairgrieve, Y. A. Kuznetsov, B. E. Oldeman, B. Sandstede, and X. J. Wang, Technical Report (Available via ftp from ftp.cs.concordia.ca/pub/doedel/auto.), California Institute of Technology, Pasadena CA91125 (2000).
28. A. Arnéodo, P. H. Coullet, and E. A. Spiegel, *Phys. Lett. A* **94**, 1-6 (1983)
29. K. Kaneko, *Prog. Theor. Phys.* **69**, 1806-1810 (1983)
30. M. Sekikawa, T. Miyoshy, and N. Inaba, *IEEE Trans. Circuits Syst. I* **48**, 28-34 (2001)
31. M. Sekikawa, N. Inaba, T. Yoshinaga, and T. Tsubouchi, *Phys. Lett. A* **374**, 187-194 (2006)
32. Yu. A. Kuznetsov , H. G. E. Meijer , L. Van Veen, *Int. J. Bifurcation & Chaos* **14**, 2253-2282 (2004)
33. S. Smale, *Bull. Am. Math. Soc.* **73**, 747-817 (1967)
34. O. V. Sosnovtseva, A. N. Pavlov, E. Mosekilde, K.-P. Yip, N.-H. Holstein-Rathlou, and D. J. Marsh, *Am. J. Physiol.* **293**, F1545-F1555 (2007)
35. D. J. Marsh, O. V. Sosnovtseva, E. Mosekilde, and N.-H. Holstein-Rathlou, N.-H., *Chaos* **17**, 15114-10 (2007)
36. J. L. Laugesen, O. V. Sosnovtseva, E. Mosekilde, N.-H. Holstein-Rathlou, and D. J. Marsh, *Am. J. Physiol.* **298**, R997-R1006 (2010)
37. H. Gustafsson, A. Bülow, and H. Nilsson, *Acta Physiol. Scand.* **152**, 145-152 (1994)
38. M. J. Davis, and M. A. Hill, *Physiol. Rev.* **79**, 387-423 (1999)
39. L. C. Moore, *Am. J. Physiol.* **247**, F267-F276 (1984)
40. N.-H. Holstein-Rathlou, and P. P. Leyssac, *Acta Physiol. Scand.* **126**, 333-339 (1986)
41. N.-H. Holstein-Rathlou, A. J. Wagner, and D. J. Marsh, *Am. J. Physiol.* **260**, F53-F68 (1991)
42. H. Gustafsson, and H. Nilsson, *Acta Physiol. Scand.* **149**, 283-291 (1993)
43. J. C. B. Jacobsen, C. Aalkjaer, V. V. Matchkov, H. Nilsson, J. J. Freiberg, and N.-H. Holstein-Rathlou, *Phil. Trans. Roy. Soc A* **366**, 3483-3502 (2008)
44. O. V. Sosnovtseva, A. N. Pavlov, E. Mosekilde, and N.-H. Holstein-Rathlou, *Phys. Rev. E* **66**, 061909-7 (2002)
45. O. V. Sosnovtseva, E. Mosekilde, A. N. Pavlov, N.-H. Holstein-Rathlou, and D. J. Marsh, *Phys. Rev. E* **70**, 031915-8 (2004)
46. N.-H. Holstein-Rathlou, *J. Am. Soc. Nephrol.* **4**, 1275-1287 (1993)
47. N.-H. Holstein-Rathlou, and D. J. Marsh, *Physiol. Rev.* **74**, 637-681 (1996)
48. N.-H. Holstein-Rathlou, and D. J. Marsh, *Am. J. Physiol.* **258**, F1448-F1459 (1990)
49. M. Barfred, E. Mosekilde, and N.-H. Holstein-Rathlou, *Chaos* **6**, 280-287 (1996)